Soft Matter

PAPER

View Article Online
View Journal | View Issue

Cite this: *Soft Matter*, 2015, **11**, 6460

Self-assembly and hybridization mechanisms of DNA with cationic polythiophene†

Jenifer Rubio-Magnieto,[a] Elias Gebremedhn Azene,[a] Jérémie Knoops,[a] Stefan Knippenberg,‡[a] Cécile Delcourt,[a] Amandine Thomas,[ab] Sébastien Richeter,[b] Ahmad Mehdi,[b] Philippe Dubois,[c] Roberto Lazzaroni,[a] David Beljonne,[a] Sébastien Clément[b] and Mathieu Surin*[a]

Received 16th June 2015,
Accepted 7th July 2015

DOI: 10.1039/c5sm01484k

www.rsc.org/softmatter

The combination of DNA and π-conjugated polyelectrolytes (CPEs) represents a promising approach to develop DNA hybridization biosensors, with potential applications for instance in the detection of DNA lesions and single-nucleotide polymorphisms. Here we exploit the remarkable optical properties of a cationic poly[3-(6′-(trimethylphosphonium)hexyl)thiophene-2,5-diyl] (**CPT**) to decipher the self-assembly of DNA and **CPT**. The ssDNA/**CPT** complexes have chiroptical signatures in the **CPT** absorption region that are strongly dependent on the DNA sequence, which we relate to differences in supramolecular interactions between the thiophene monomers and the various nucleobases. By studying DNA–DNA hybridization and melting processes on preformed ssDNA/**CPT** complexes, we observe sequence-dependent mechanisms that can yield DNA-condensed aggregates. Heating–cooling cycles show that non-equilibrium mixtures can form, noticeably depending on the working sequence of the hybridization experiment. These results are of high importance for the use of π-conjugated polyelectrolytes in DNA hybridization biosensors and in polyplexes.

Introduction

Within the family of π-conjugated polyelectrolytes (CPEs), cationic polythiophenes (**CPT**) hold great promise in the development of biosensors for genomics and proteomics, noticeably for the detection of DNA hybridization and the amyloid fibril formation.[1–8] The solubility of cationic polythiophene in aqueous media and the remarkable optical properties as a result of the molecular wire effect make this compound suitable for sensitively probing the interactions with DNA, which possesses a negatively-charged phosphodiester backbone and binds with **CPT** primarily through electrostatic interactions.[9] The optical signature of the binding process of **CPT** with DNA, such as fluorescence amplification, has been exploited for the determination of very low concentrations of DNA,[10–13] for protein identification using **CPT**/DNA aptamer complexes,[14] and for the fabrication of new DNA biochips.[4] Remarkably, a series of **CPT** (and other CPE)-based optical biosensors able to report DNA–DNA or DNA–PNA hybridization have been described in the literature, with promising applications in the detection of Single-Nucleotide Polymorphism (SNP) and in the identification of neurodegenerative diseases.[2,5,11,12,15–19] The principle of these hybridization biosensors, as introduced by Heeger, Bazan, Leclerc and their colleagues, is that the CPE fluorescence is quenched when the polymer chain is bound to a single-stranded DNA, while the fluorescence is recovered or amplified only in the presence of the complementary strand, which can bear a fluorophore dye to exploit Fluorescence Resonance Energy Transfer (FRET).[12,15,20,21] Recently, Leclerc *et al.* pointed out that the fluorescence signal, and therefore the detection sensitivity of label-free DNA/**CPT** hybridization biosensors (*i.e.* without dye appended on the complementary DNA strand), is strongly dependent on the nature of the DNA sequences to hybridize.[22] For other single-stranded DNA/CPE complexes, it was also observed that the photoluminescence properties of CPEs depend on the DNA sequence.[23] This is interpreted as a direct consequence of the different conformational changes and binding mechanisms of **CPT** with various DNA sequences,

[a] *Laboratory for Chemistry of Novel Materials, Center for Innovation in Materials and Polymers, University of Mons – UMONS, 20 Place du Parc, B-7000 Mons, Belgium. E-mail: mathieu.surin@umons.ac.be; Tel: +32 65373868*
[b] *Institut Charles Gerhardt ICGM, UMR 5253 CNRS-ENSCM-UM, Université de Montpellier – CC1701, Place Eugène Bataillon, F-34095 Montpellier Cedex 05, France*
[c] *Laboratory for Polymeric and Composites Materials, Center for Innovation in Materials and Polymers, University of Mons – UMONS, 20 Place du Parc, B-7000 Mons, Belgium*

† Electronic supplementary information (ESI) available: Preparation of oligonucleotides and DNA/**CPT** mixtures, additional UV-Vis, CD, and fluorescence spectra; additional AFM images; methodology and figures of molecular modelling simulations. See DOI: 10.1039/c5sm01484k

‡ Present address: Division of Theoretical Chemistry & Biology, School of Biotechnology, KTH Royal Institute of Technology, SE-10691 Stockholm, Sweden.

affecting the homogeneity of the assays. However, the structures formed upon DNA/CPE complexation, and the effects of the sequence, length, and topology of the DNA on the hybridization mechanism and the supramolecular assembly remain virtually unexplored, which constitutes a strong limitation in the understanding of the detection (selectivity and sensitivity) properties and is a requisite to rationally design reliable and stable biosensors. Besides, an in-depth understanding of the self-assembly mechanisms is required to further develop DNA/**CPT** nanomaterials for biomedical applications, as DNA/**CPT** nanomaterials are also envisioned for the regulation of gene expression and as polyplexes for non-viral gene delivery.[24–26]

In this context, we recently reported on the design of a series of achiral cationic polythiophenes that assemble with nucleic acids into hybrid complexes to form chiral supramolecular structures.[27] We showed that the chirality of the self-assembled DNA/polythiophene structures is notably affected by the nature of the polymer cationic side groups: in particular, polythiophenes with charge-localized cationic groups, such as quaternized ammonium or phosphonium (see Chart 1), show upon DNA binding specific induced circular dichroism (ICD) signatures in the polymer band, which relate to the polymer preferential chiral conformation in the complex. Especially, the cationic poly[3-(6′-(trimethylphosphonium)hexyl)thiophene-2,5-diyl] (**CPT**) shows strong ICD signals in the π–π* band when it is mixed to DNA in aqueous solutions, and we observed that the DNA sequence has important effects on these chiroptical signals. Noticeably, left-to-right transitions in the helical assembly of the polymer occur as a function of various factors, such as the molar ratio and the temperature.

In the work reported here, we exploit these remarkable properties to probe the effects of the DNA sequence, topology, and length on the self-assembly of DNA/**CPT** in hybridization experiments in solution, as a requisite to understand the detection properties in **CPT**-based biosensors and to develop DNA/**CPT** polyplexes. Three important processes for the functioning of hybridization biosensors are examined:

(i) *Complexation*: the formation of a complex between the cationic polymer and the anionic DNA, whatever its topology, for single-stranded DNA (ssDNA) or double-stranded DNA (dsDNA);

(ii) *Hybridization*: the hybridization of complementary DNA sequences (DNA double-helix formation) on a preformed ssDNA/**CPT** complex;

(iii) *Melting*: DNA melting temperature studies to follow the de-hybridization (melting) and re-hybridization processes in dsDNA–polymer complexes obtained in the hybridization experiments. By studying a series of complementary DNA probes, differing by the purine/pyrimidine base ratio, we reveal how the DNA/**CPT** self-assembly is influenced by the DNA sequence. The combination of UV-Vis absorption, circular dichroism, and fluorescence spectroscopies, atomic force microscopy, and molecular modelling simulations provides important clues on the structures formed in DNA/**CPT** complexes, which are helpful for future developments of DNA hybridization biosensors and CPE-based polyplexes.

Results and discussion

Cationic polythiophene **CPT** (Chart 1) was synthesized as previously reported.[27] **CPT** has a number-averaged molecular weight (M_n) of 17 700 g mol^{-1} as estimated from the monomodal trace of the **P3HT-Br** precursor in GPC ($M_n \sim 13\,500$ g mol^{-1}, $Đ = 1.27$), which is in fair agreement with MALDI-ToF mass spectrometry measurements (estimated $M_n \sim 11\,500$ g mol^{-1}).[27,28] At the concentrations used in this study (typically a few μM), **CPT** is molecularly dissolved in water or in methanol solutions, as deduced from the fact that no signature of aggregation is observed in absorption UV-Vis spectra (see Fig. S1†). The signatures of the **CPT** aggregation, *i.e.* a red-shift of the UV-Vis spectrum (up to a maximum absorption wavelength around 550 nm) and the appearance of a characteristic shoulder at around 600 nm,[29] are observed only upon addition of THF to the water (or methanol) solutions, THF being a poor solvent for the studied cationic polythiophene.

The formation of DNA/**CPT** complexes and the effect of DNA/DNA hybridization were studied in aqueous buffered solutions by mixing **CPT** with selected DNA oligonucleotide probes possessing complementary sequences, see Chart 2. These oligonucleotide (ODN) sequences are selected because they represent model cases: **dT** is a homopyrimidine ODN, **dA** is a homopurine ODN, and both **dR** and **dR$_{rev}$** ODNs possess a mixed sequence, each with half purines and half pyrimidines. Note that guanine-rich oligonucleotides were excluded in the frame of this study because of their propensity to form unusual secondary structures, such as intramolecular G-quadruplexes.[30] The length of the oligonucleotides has been optimized based

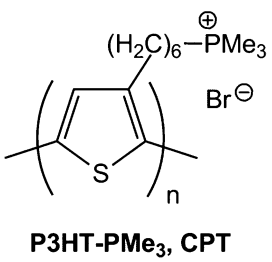

P3HT-PMe$_3$, CPT

Chart 1 Chemical structure of the cationic poly[3-(6′-(trimethylphosphonium)hexyl)thiophene-2,5-diyl], hereafter named **CPT**.

ssDNA

d(T)$_{20}$: 5'- TTT TTT TTT TTT TTT TTT TTT TT-3', **dT$_{20}$**

d(A)$_{20}$: 5'-AAA AAA AAA AAA AAA AAA AA-3', **dA$_{20}$**

d(T)$_{40}$: 5'- TTT TTT TTT TTT TTT TTT TTT TTT TTT TTT TTT TTT TTT TTT T-3', **dT$_{40}$**

d(A)$_{40}$: 5'-AAA AAA AAA AAA AAA AAA AAA AAA AAA AAA AAA AAA AAA A-3', **dA$_{40}$**

d(R)$_{20}$: 5'-CGT CAC GTA AAT CGG TTA AC-3', **dR$_{20}$**

d(R)$_{rev20}$: 5'-GTT AAC CGA TTT ACG TGA CG-3', **dR$_{rev}$**

d(R)$_{43}$: 5'-CGT CAC GTA AAT CGG TTA ACA AAT GGC TTT CGA AGC TAG CTT C-3', **dR$_{43}$**

dsDNA

d(A)$_{20}$d(T)$_{20}$: 5'-AAA AAA AAA AAA AAA AAA AA-3' / 3'- TTT TTT TTT TTT TTT TTT TT-5', **dA·dT**

d(R)$_{20}$d(R)$_{rev20}$: 5'-CGT CAC GTA AAT CGG TTA AC-3' / 3'-GCA GTG CAT TTA GCC AAT TG-5', **dR·dR$_{rev}$**

Chart 2 Sequences of the DNA oligonucleotides (ODN).

on our earlier results,[27] to achieve approximately a neutral charge balance when **CPT** (with an average of 47 monomer units in the chains, from $\langle M_n \rangle$) is complexed to the longer single-stranded DNA (40 bases) or when it is complexed to a double-stranded DNA with two 20-base-pairs (bp) strands. For each ODN shown in Chart 2, (chir)optical spectroscopy (UV-Vis absorption, circular dichroism, and fluorescence) was used to examine the three aforementioned processes described here with their terminology: (i) *Complexation*: the formation of a complex (or polyplex) between a single-stranded DNA and **CPT** (*e.g.* **dT/CPT**, see Chart 2) or between a double-stranded DNA and **CPT** (*e.g.* **dA·dT/CPT**, Chart 2); (ii) *Hybridization*: a ssDNA/**CPT** complex on which the complementary DNA strand is added, *e.g.* **dT/CPT + dA**. This hybridization is compared to the formation of a complex between a pre-formed double-stranded DNA and **CPT**, which can be viewed as the formation of a 'triplex' structure between the two DNA strands and the polymer chain;[3,31] (iii) *Melting*: variable-temperature experiments on DNA/**CPT** polyplexes, compared to the melting properties of the pure DNA double helix. Note that except for the melting experiments, all the measurements were carried out at 20 °C, using a DNA concentration of ~7 μM in TE buffer (pH = 7.4) and the solutions were left to equilibrate for 30 minutes before the spectroscopic measurements.

Complexation of ssDNA/CPT

CPT was mixed with single-stranded ODN (listed in Chart 2) at a 1 : 1 molar ratio in a TE buffer solution at pH 7.4, yielding solutions of ssDNA/**CPT** complexes. The solutions were equilibrated for 30 minutes, after which UV-Vis absorption spectra show no change (see stability tests in ESI†). For each ssDNA : **CPT** mixture, the UV-Vis absorption measurements show large red-shifted absorption maxima compared to λ_{max} of the pure polymer **CPT**, as listed in Table 1, with identical shifts $\Delta\lambda_{max}$ = +46 nm for all mixtures with the longer ssDNA (**dT$_{40}$**, **dA$_{40}$**, and **dR$_{43}$**). Given the hydrophobic nature of the π-conjugated backbone, the **CPT** chains are most probably folded in water, with the cationic substituents exposed to the aqueous medium. Upon interaction with ssDNA, the **CPT** chain unfolds to a more planar conformation, *i.e.*, a more π-conjugated backbone, consistent with the red-shifted absorption. Although the position of the λ_{max} is not linearly correlated with the concentration of **CPT** in solutions of ssDNA/**CPT** complexes, the extent of red-shift (and therefore the color of the solution) depends on the ssDNA/**CPT** composition, as shown in Fig. 1 and Fig. S6.† In Fig. 1b is plotted the shift in **CPT** UV-Vis maximum absorption ($\Delta\lambda_{max}$, relative to λ_{max} of the pure polymer) as a function of composition in **CPT** in a **dR$_{20}$: CPT** mixture, keeping constant the total concentration of **CPT** and DNA. A maximum red-shift is observed at a composition of ~0.4, beyond which the red-shift starts to decrease. This value is approximately the charge ratio of negative to positive charges ($R_{-/+}$), as estimated with the 20 negative charges of **dR$_{20}$** and an average of 47 cationic groups in **CPT** (estimated from $\langle M_n \rangle$ obtained by MALDI-ToF experiments).[27,28] This observation indicates that

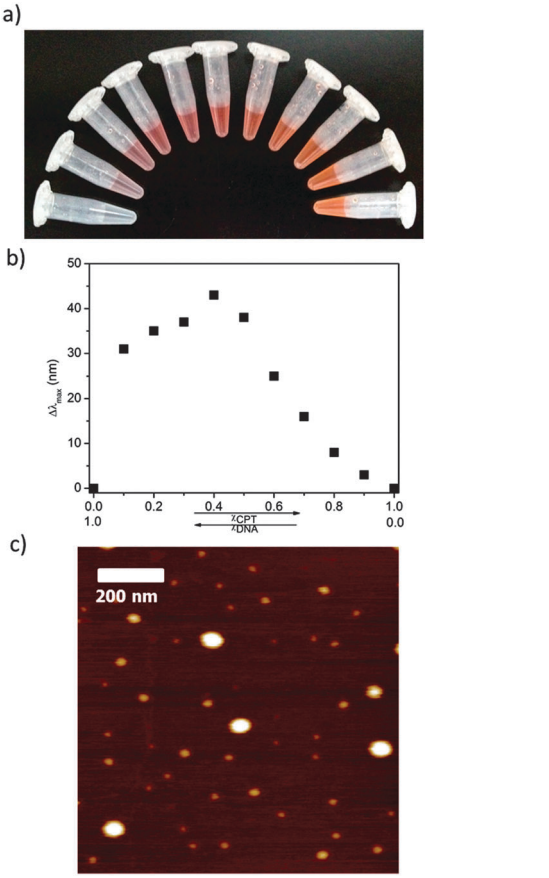

Fig. 1 (a) Pictures of the **dR$_{20}$: CPT** mixtures at various compositions of a dR$_{20}$: **CPT** mixture, with χ**CPT** = 0 to χ**CPT** = 1 from the left to the right (χ**CPT** = mole fraction of the polymer; total concentration $C_{\mathbf{dR20}}$ + $C_{\mathbf{CPT}}$ = 8.5 μM, in TE buffer). (b) Plot of UV-Vis $\Delta\lambda_{max}$ (compared to pure **CPT**) at various compositions shown in (a). (c) AFM height image (1.0 × 1.0 μm^2) of a thin deposit of **dR$_{43}$/CPT** on mica (vertical height scale: 6 nm).

Table 1 UV-Vis maxima absorption wavelength (λ_{max}) and shifts ($\Delta\lambda_{max}$) of DNA/**CPT** mixtures

	UV band		Vis band	
Complex[a]	λ_{max} (nm)	$\Delta\lambda_{max}$[b]	λ_{max} (nm)	$\Delta\lambda_{max}$[c]
dT$_{20}$/CPT	268	+4	494	+43
dT$_{40}$/CPT	268	+3	497	+46
dT$_{20}$/CPT/dA$_{20}$	259	−5	477	+26
dA·dT/CPT	266	+6	473	+22
dA$_{20}$/CPT	269	+12	442/520[d]	−9/+69[d]
dA$_{40}$/CPT	259	+3	497	+46
dA$_{20}$/CPT/dT$_{20}$	267	+10	469	+18
dR$_{20}$/CPT	261	+4	495	+44
dR$_{43}$/CPT	261	+2	497	+46
dR$_{20}$/CPT/dR$_{rev20}$	260	+3	494	+43
dR·dR$_{rev}$/CPT	262	+5	493	+42
dR$_{rev20}$/CPT	261	+4	490	+39
dR$_{rev20}$/CPT/dR$_{20}$	260	+3	491	+40

[a] Measured at 20 °C in TE buffer (pH 7.4) at 1 : 1 or 1 : 1 : 1 molar ratio, ([DNA]) ~7 μM. [b] Considering λ_{max} (**dT$_{20}$, dT$_{40}$, dA·dT, dA$_{20}$, dA$_{40}$, dR$_{20}$, dR$_{43}$, dR$_{rev20}$**, and **dR·dR$_{rev}$**) = 264, 265, 260, 257, 256, 257, 259, 257 and 257 nm, respectively. [c] Considering λ_{max} (**CPT**) = 451 nm. [d] UV-Vis spectrum of **dA$_{20}$/CPT** shows a maximum intensity λ_{max} at 442 nm with a large shoulder at around 520 nm, see ESI.

the extent of the red-shift in λ_{max} (due to unfolding/planarization of the polymer chains upon DNA binding) is related to the charge ratio $R_{-/+}$, likely ruling the stoichiometry of the self-assembly. Note that for **dA_{20}/CPT**, the UV-Vis experiments show a very large red-shift of the absorption maximum up to a 1 : 0.4 **dA_{20} : CPT** molar ratio, up to $\Delta\lambda_{max} \sim +70$ nm. However, above a molar ratio of 1 : 0.6, λ_{max} gradually shifts back towards lower wavelengths, eventually yielding a slightly blue-shifted absorption maximum at a 1 : 1 molar ratio, but with a very large shoulder still present in the 500–550 nm region (Fig. S7†). However, the complexation of **CPT** with longer sequences (**dA_{40}**) yields a red-shifted absorption maximum whatever the molar ratio in the 1 : 0.2 to 1 : 1 range (**dA_{40} : CPT**, Fig. S7†), which altogether indicates the importance of the charge balance in the self-assembly process.

The size of DNA/π-conjugated polyelectrolytes complexes in aqueous solution strongly depends on the concentration and the solution composition.[32,33] For the ssDNA/**CPT** complexes studied here at charge ratio $R_{-/+} \sim 1$, atomic force microscopy (AFM) of thin deposits on mica substrates shows structures with nanometer-scale dimensions. Fig. 1c shows an AFM image of a deposit of **dR_{43}/CPT**, revealing round-shaped objects characterized by a width from around 5 nm for the smallest ones to around 50 nm for the few largest ones (taking into account tip lateral convolution effects) and a small thickness ranging from 1 nm to around 5 nm. Note that structures of rather similar shape and sizes were observed by AFM for other complexes drop-cast also from pure water solutions, with some larger structures possibly due to the aggregation of smaller structures upon solvent evaporation, but in all cases the objects have a nm-scale thickness (Fig. S8†). The size of these structures is indicative that rather small polyelectrolyte complexes are formed under our solution conditions, *i.e.*, from bimolecular ssDNA/**CPT** complexes for the smallest structures (in agreement with a radius of gyration between 2 and 4 nm, as estimated for molecular modelling, see below) to clusters comprising a few tens of molecules for the largest structures, probably *via* inter-polyelectrolyte aggregation. Note that Bazan *et al.* have studied the growth characteristics of another type of cationic copolymers and ssDNA, and they showed that small inter-polyelectrolyte aggregates, with sizes between 5 and 10 nm, are formed at a comparable charge ratio and polymer concentration.[33]

The differences observed in UV-Vis absorption spectra for the different complexes prompted us to carry out circular dichroism (CD) experiments. For **dT_{20}/CPT** we observe a (+/−) bisignate induced CD signal (ICD) in the region where the polymer absorbs (Fig. 2c). This ICD is the signature of a helical conformation of the polymer chain in the ssDNA/**CPT** complex, as also observed for complexes of anionic PT and cationic peptides, for oligothiophene–proline amino acid conjugates, and for hydrogen-bonded DNA/oligo(*para*-phenylene vinylene) self-assembled structures.[34–36] For **dT_{20}/CPT**, the sign of the ICD is attributed to a preferential right-handed helical conformation of the polymer within the **dT/CPT** complex.[27] The same behavior is observed for the longer single-stranded DNA (**dT_{40}**), with a higher intensity in the (+/−) ICD band in the region where **CPT** absorbs (Fig. 2c). This indicates that the single-stranded DNA acts as a template to organize the polymer chain in a preferential chiral conformation. In contrast, for **dA_{20}/CPT**, there is no ICD signal in the polymer region at any molar ratio.

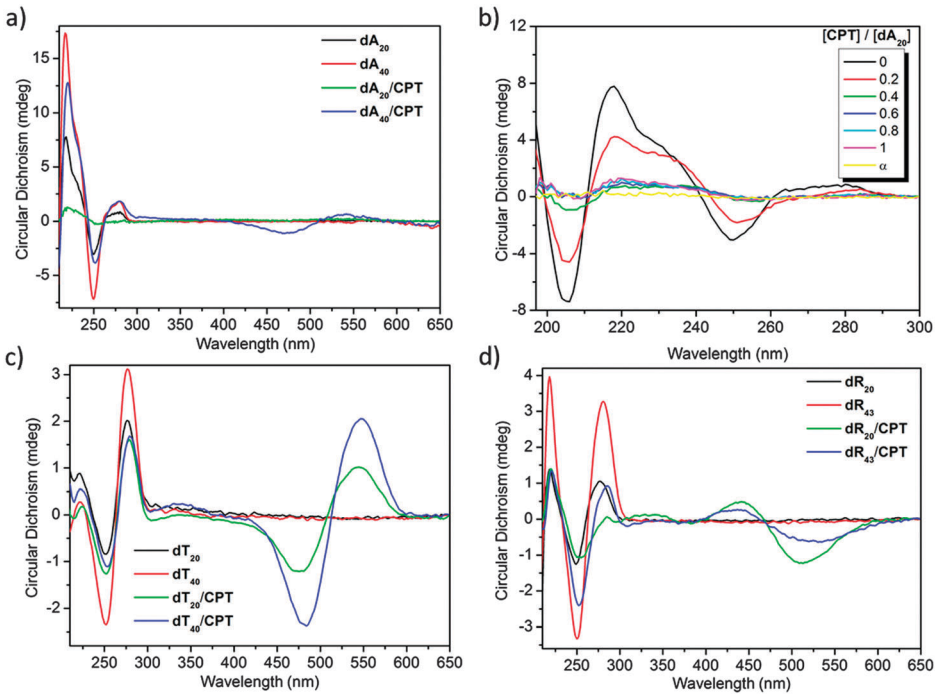

Fig. 2 Circular Dichroism (CD) spectra of several ssDNA/**CPT** mixtures at a 1 : 1 molar ratio at 20 °C in TE buffer: (a) **dA/CPT**; (b) the effect of the **CPT** concentration on the CD spectra of **dA_{20}/CPT** in the 190–300 nm region; (c) **dT/CPT**; and (d) **dR/CPT**.

For **dA$_{40}$/CPT**, we observe a (+/−) ICD signal in the polymer region, but weaker than for **dT$_{40}$/CPT** complexes (Fig. 2a). Note that, in the case of **dA$_{20}$/CPT** complexes, the CD signal in region 210–300 nm is gradually flattened upon addition of the polymer, compared to that of pure **dA** (Fig. 2b and Fig. S9 and S10†). **CPT** also absorbs in this region, therefore the changes in CD spectra below 300 nm cannot be attributed exclusively to changes in the CD signals of DNA. However, only for the case of **dA/CPT** the changes in the CD signal in this region are so important. Altogether with UV-Vis experiments, this may indicate a strong binding between **dA** and **CPT**, which significantly distorts the right-handed **dA** helix in solution,[37] as confirmed by modelling (see below).

For **dR$_{20}$/CPT**, **dR$_{rev20}$/CPT**, and **dR$_{43}$/CPT** complexes, we observe bisignate (−/+) ICD signals in the polymer region, characteristic of a preferential left-handed helical chirality (Fig. 2d). We observe changes in the CD signal in the range 210–300 nm: the positive band at 275 nm decreases and there is a red-shift of the negative band at 245 nm in comparison with pure **dR$_{20}$**, **dR$_{rev20}$**, and **dR$_{43}$**. Therefore, the CD signals of mixed sequences (**dR$_{20}$** or **dR$_{rev20}$**) complexed with **CPT** are intermediate between the two homonucleotide sequences: in this case the **CPT** disturbs the DNA conformation, in contrast to what happens with **dT$_{20}$**, but not as much as in the case of **dA$_{20}$**. Altogether, this shows that the conformational reorganization of the polymer chain upon ssDNA binding is sequence- and length-dependent, with distinct behaviors for homopyrimidine DNA ((+/−) ICD for both **dT$_{20}$** and **dT$_{40}$**), mixed purine/pyrimidine DNA ((−/+) ICD for both **dR$_{20}$** and **dR$_{43}$**), and homopurine (no ICD and (+/−) ICD, for **dA$_{20}$** and **dA$_{40}$**, respectively), which attests that monomer-base interactions are critical in the self-assembly.

Complexation of dsDNA/CPT

In the case of the binding of **CPT** with preformed double-stranded DNA **dA·dT** (oligonucleotide duplex) at a 1 : 1 molar ratio, the UV-Vis spectra indicate a smaller red-shifted absorption maximum of the polymer ($\Delta\lambda_{max}$ ∼ +22 nm) than for complexes with the corresponding single-stranded DNA **dT** (Table 1 and Fig. S11†). The CD signals of **dA·dT/CPT** show that characteristic CD bands for the double-stranded DNA (duplex) are maintained, and no ICD effect appears in the polymer band (Fig. 3a). Therefore, the binding with the polymer barely affects the double-helical structure of the **dA·dT** duplex.

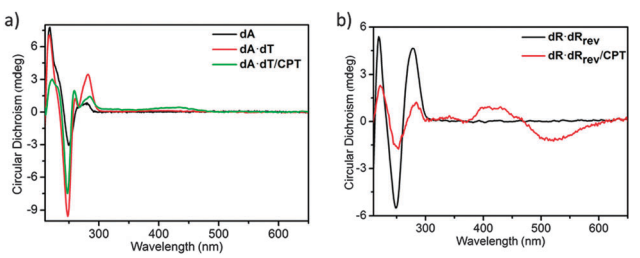

Fig. 3 (a) CD spectra of **dA** (black line), **dA·dT** (red line) and **dA·dT/CPT** (green line) at a 1 : 1 molar ratio; and (b) CD spectra of **dR·dR$_{rev}$** (black line) and **dR·dR$_{rev}$/CPT** (red line) at a 1 : 1 molar ratio.

This is probably due to the unlikeliness of π–π interactions between **CPT** chains and dsDNA (see below), and the related lower hydrophobicity of the dsDNA duplex compared to ssDNA.[9]

In contrast, for the **dR·dR$_{rev}$/CPT** binding, the UV-Vis spectrum shows a marked red-shift of the absorption maximum ($\Delta\lambda_{max}$ ∼ +42 nm), rather similar to that in **dR/CPT** or **dR$_{rev}$/CPT** ($\Delta\lambda_{max}$ ∼ +44 nm and +39 nm, respectively), which indicates that the red-shift of the absorption maximum is not simply related to the charge balance (see Table 1 and Fig. S12†). For the **dR·dR$_{rev}$/CPT** complexes, the CD spectra show a decrease in the intensity of the characteristic B-DNA bands (Fig. 3b), which may indicate a lower extent of coupling between base pairs within the helix, probably due to base flipping upon **CPT** binding,[38] and a bisignate (−/+) ICD signal with a zero-crossing around 474 nm, as in the case of **dR/CPT** (Fig. S12†). The sign of the ICD again suggests that either the polymer chain surrounds the DNA duplex preferentially in a left-handed conformation or that there is a preferential left-handed helical assembly of **CTP** chains (aggregation effect) while the complex is forming. This prompted us to carry out molecular modelling simulations of the DNA/**CPT** complexes, to understand the possible binding modes upon complexation.

Structures of DNA/CPT complexes: molecular modelling

To get insights into the supramolecular interactions and structures involved in the complexation of **CPT** with the different DNA strands, an atomistic molecular modelling study was performed by means of Molecular Dynamics (MD) simulations in an implicit water solvent model, see methodology in the ESI.† The modeled structures represent the initial steps of complexation of one DNA strand (either ssDNA or dsDNA) with one **CPT** polymer chain, in order to elucidate the monomer-base interactions and the conformational rearrangements of each partner upon complexation, in connection with the (chir)optical properties. Aggregates of several DNA chains with several **CPT** chains were not investigated because of the too high computational cost associated with the large number of possible arrangements. Three sets of MD simulations were performed: (i) complexation of **CPT** with the single-stranded DNA **dA$_{20}$** or **dT$_{20}$**; (ii) the assessment of preferential sites of **CPT** interaction along double-stranded DNA, **dA·dT** and **dR·dR$_{rev}$**, and (iii) the role of the length of the polymer chain in the formation of a helical structure upon complexation with double-stranded DNA.

Modelling of ssDNA/CPT complexes. We here assess the possible structural differences between **dA/CPT** and **dT/CPT** complexes, which represent the two extreme cases in terms of sequence (**dA** is a homopurine strand whereas **dT** is a homopyrimidine strand). Starting from several initial conformations, complexes with a helicoidal **CPT** chain made of 40 thiophene units (*i.e.* close to the average degree of polymerization) around ssDNA (20 bases) were selected, see details in the ESI.† Our approach is to check whether structural arrangements that are congruent with the measured spectroscopic data (namely the CD response, hence the selection of helicoidal conformations) are plausible. This is achieved by comparing their relative energy

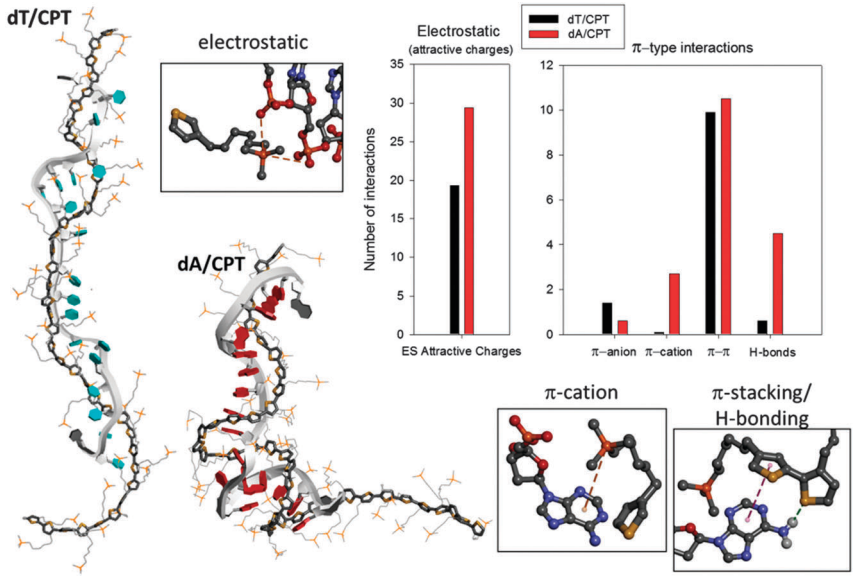

Fig. 4 Left: Snapshots of **dT/CPT** and **dA/CPT** complexes extracted at the end of the MD simulations. The polythiophene backbone is shown as thick sticks, the thymine and adenine nucleobases in blue and red, respectively, and the DNA backbone as a gray ribbon. Details of some intermolecular interactions are shown in the boxes. Top right: Plots of the average number of intermolecular interactions for the two complexes, as estimated by averaging ten snapshots on the last nanosecond of the MD run.

and stability with respect to small excursions in the valleys around the local minima on the potential energy surfaces, as sampled along the MD runs. By performing MD runs for 15 ns at 300 K, we observe structural differences between the two types of complexes (**dA/CPT** and **dT/CPT**), as illustrated in the final MD snapshot (Fig. 4). Along the MD simulations, we noticed that the **dT** and **CPT** backbones tend to become extended, see snapshots in Fig. 4. In contrast, for the **dA/CPT** complex, the **dA** strand tends to condense while the **CPT** chain coils around it, which ultimately leads to a more compact, intertwined complex. This is also observed by following the changes in the radius of gyration (R_g) of both the polymer and the ssDNA strand over the course of the MD, as plotted in Fig. 5a. Both R_g of DNA and that of **CPT** in the **dT/CPT** complex show an overall increase, while those in the **dA/CPT** complex show a clear decreasing trend, which indicate stretching and condensation of the complexes, respectively. The root-mean-square deviation (RMSD) of the two complexes along the MD shows that the structural changes undergone by the **dA/CPT** complex are larger than those in the **dT/CPT** complex (see ESI†).

The favorable intermolecular interactions were estimated and averaged from ten snapshots over the last nanosecond of the MD simulations, as plotted in Fig. 4. The electrostatic (attractive charges) between the polymer phosphonium groups and the DNA phosphate groups are far more numerous in average for **dA/CPT** (around 30) than for **dT/CPT** (around 20), because of the more compact assembly in the former. An example of these interactions is depicted in the box at the top of Fig. 4. Besides, π-type interactions (especially π-cations) are globally more frequent in **dA/CPT**, which makes sense in view of the more extended π-conjugated plane of the Adenine base compared to the Thymine base. In addition, weak S(thiophene)–H(guanine amino) hydrogen-bonds can form in **dA/CPT** to a larger extent than in **dT/CPT**, see Fig. 4 right. Altogether, the calculations indicate a larger number of interactions between **CPT** and DNA in **dA/CPT** compared to **dT/CPT**. To assess the difference in interaction energies, the binding free energies between **CPT** and DNA were calculated from the MD simulations in the MM/GBSA approach. The average difference in binding free energy $\Delta\Delta G_{\mathrm{GBSA}}$ amounts to $\sim$53 kcal mol^{-1} in favor of the **dA/CPT** complex (*i.e.*, **dA/CPT** is more strongly bound than **dT/CPT**). This again supports the view that **dA/CPT** has stronger intermolecular interactions than **dT/CPT**, in line with the experimental observations.

Fig. 5b represents the evolution of the average and standard deviations of a DNA local chirality index, as obtained from 15 ns MD simulation runs in **dA/CPT** and **dT/CPT** complexes. This index is defined as the following dimensionless scalar triple product:

$$\mathrm{ind}(i,j) = \frac{\vec{r}_{ij} \cdot \vec{\mu}_i \times \vec{\mu}_j}{|\vec{r}_{ij}||\vec{\mu}_i||\vec{\mu}_j|}$$

where $\vec{\mu}_i$ and $\vec{\mu}_j$ denote two vectors oriented in the plane of nearest neighbor A (or T) bases and $\vec{r}_{ij}$ is a vector connecting their geometric centers. The average local chirality of the DNA in both the **dA/CPT** and **dT/CPT** complexes is positive, consistent with a right-handed DNA helical structure, and decreases during the simulations, due to deviation from the idealistic helical arrangement present in the starting simulation structures. However, these deviations are far larger in the case of **dA/CPT** than in the case of **dT/CPT**, both in terms of the average value and standard deviation, suggesting a stronger interaction with

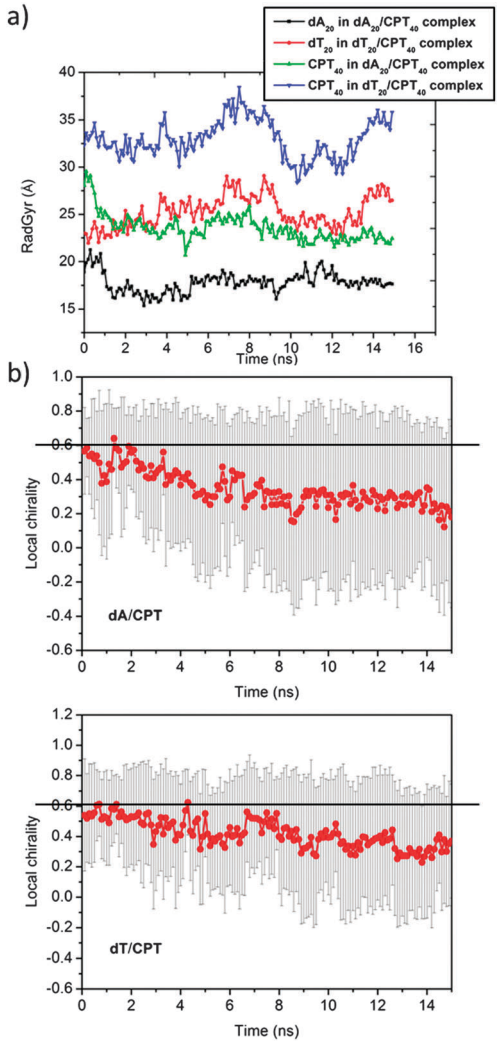

Fig. 5 (a) Evolution of the radius of gyration (in Å) for the DNA strands and the polymer chain in the **dA$_{20}$/CPT40** complexes along the MD simulation. (b) Evolution of the average (red circles) and standard (bars) deviations of the DNA local chirality index for **dA/CPT** (top) and **dT/CPT** (bottom) complexes along the MD simulation.

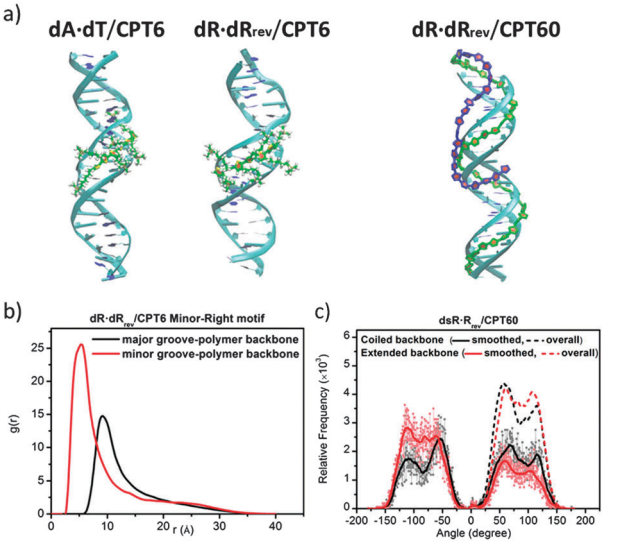

Fig. 6 (a) Snapshots of the final structures of MD simulated **dsDNA/CPT** complexes, from the minor-groove configurations. In the snapshot shown on the right with CPT60, the coiling around DNA is shown in green, while the part of the polymer chain that was left to hang in to the solvent environment in the initial structure is shown in blue (only the polymer backbone is shown for the sake of clarity). (b) Radial distribution functions of the polymer backbone atoms in relative minor grooves of **dR·dR$_{rev}$** in **dsDNA/CPT6** complexes. (c) Distribution of the dihedral angles between adjacent thiophene rings in **dR·dR$_{rev}$/CPT60** complexes. The dashed lines show the sum of positive and negative dihedral angles.

the polymer chain for **dA/CPT**. This is in agreement with the ICD signatures for both **dT/CPT** and **dA/CPT**, showing a right-handed conformational assembly of the polymer chain around the ssDNA template, and upon complexation a large change in the CD signatures of **dA** (Fig. 2a and b), while the CD bands of **dT** show only a smaller intensity change (Fig. 2c).

Modelling of dsDNA/CPT complexes. The grooves of double-stranded DNA are known to constitute interaction sites for cationic macromolecules. Groove-binding events may lead to induced structural effects ranging from perturbation of the DNA conformation to DNA bending or kinking. In the modelling study, we started from different alignments of a small **CPT** oligomer made of 6 monomer units (hereafter named CPT6) with respect to dsDNA to follow the positional and conformational reorganization of the polymer chain during the MD simulations, see initial conformations in the ESI.† We find that for both left-handed and right-handed **CPT** starting configurations, in most cases, CPT6 slides or reorients to accommodate along the minor groove, rather than along the major groove or across the grooves (see ESI†). Even starting from a left-handed conformation, where it was initially closer to the major-groove, the polymer chain re-orients during the MD run to be in close contact with the minor groove, eventually yielding a right-handed conformation. Snapshots of the resulting structures are shown in Fig. 6a for both **dA·dT**/CPT6 and **dR·dR$_{rev}$**/CPT6. The radial distribution function of CPT6 relative to the DNA major groove or minor groove, as represented in Fig. 6b (see description in the ESI†), shows that CPT6 lies in closer contact to DNA when bound to the minor groove compared to the major groove, which indicates a stronger interaction in this site.

This is supported by estimates of the binding free energies between CPT6 and dsDNA in the complex, as calculated from the MD simulations in the MM/GBSA approach (see Table in the ESI†), indicative of a preference for a right-handed conformation along the minor-groove of dsDNA. We expect that the preference for the minor groove would be even clearer with the use of an explicit solvent model, in which the entropic contribution from the displacement of ordered water molecules within the minor groove would be accounted for.[39,40]

This preferential complexation along the minor-groove is due to both the size of the oligothiophene backbone and the position/length of the cationic lateral (trimethylphosphonium) hexyl groups, which interact with each strand of dsDNA *via* electrostatic interactions (Fig. 6a). To further assess whether

long **CPT** chains can also adopt such a type of conformation, we have simulated dsDNA/CPT60 complexes, *i.e.*, one chain made of 60 thiophene units binding to a 20 bp DNA. The simulations show that longer **CPT** chains can bind in a coiled conformation around the entire length of a 20 bp DNA, forming a two-fold helix around the DNA, *i.e.*, the pitch in the polymer chain is of 20 thiophene units per B-DNA turn (10 bp), see Fig. 6a right. Hence, for a CPT60 chain, about 40 thiophene units will wrap around the 20 bp DNA strand (depicted in green rings in Fig. 6a right) while the remaining segment (depicted in blue rings), representing one third of the chain, can either hang in the solvent environment or fold back to interact with the main body of the complex, forming a second round coiling around DNA, as shown in Fig. 6a right for **dR·dR$_{rev}$/CPT60**. Note that, in the simulated structures of dsDNA/CPT60, neighbouring thiophene units show both *cis* and *trans* types of conformation along the polymer chain, with a slight preponderance of the *cis* conformation. This is depicted in Fig. 6c, which shows a plot of the distribution of dihedral angles between adjacent thiophene units along the CPT60 backbone, with peaks at around 65° (distorted *cis*) and at around 110° (distorted *trans*) for both extended and the coiled parts of the chain.

Even though reaching equilibrium structures of DNA/**CPT** would need much longer simulation time not accessible by current state-of-the-art atomistic MD, these molecular modelling simulations provide insights into the monomer–nucleobase interactions and the structure of the complexes involved in the first steps of the complexation. The (chir)optical properties of ssDNA/**CPT** are in line with the MD results, showing larger interactions for **dA/CPT**, in which the initial **dA** helical conformation in solution becomes significantly distorted.[37] However, the proposed preferential conformation along the minor groove does not allow us to elucidate the (chir)optical behavior reported for dsDNA/**CPT**, especially for **dR·dR$_{rev}$/CPT** complexes, which show (−/+) ICD signals. We hypothesize that the aggregation of the **CPT** chains around (possibly multiple) dsDNA occurs in a particular left-handed assembly with conformational rearrangements of the DNA. Unfortunately, simulations of such aggregates would require a formidable computational effort, given the huge number of possible arrangements. This question could possibly be tackled only by combining atomistic MD and coarse-grain modelling, which is beyond the scope of this study.

Hybridization: from complexes to DNA duplex formation

The working principle of the DNA–CPE hybridization biosensors (dye labeled or label-free) is that the fluorescence of the CPE is quenched when the polymer binds to ssDNA, because chain planarization upon interaction with DNA favors the aggregation of CPE chains, leading to a non-radiative excited state. The fluorescence is recovered only in the presence of the complementary strand, when the two DNA strands hybridize.[22] Note that the selectivity of these biosensors has been studied in detail by other groups in dye-labeled DNA hybridization biosensors. It was shown that a single base pair mismatch can be detected by exploiting FRET between ssDNA/CPE and the complementary ssDNA end-capped with a dye or an intercalating dye, or their combination.[2,3,19,20,31,41] Here, fluorescence spectroscopy measurements are carried out to probe the hybridization mechanisms in a label-free biosensor configuration on both homonucleotides and random sequences (Fig. 7). The fluorescence response of ssDNA/**CPT** polyplexes is compared to the fluorescence of the pure polymer at the same concentration.

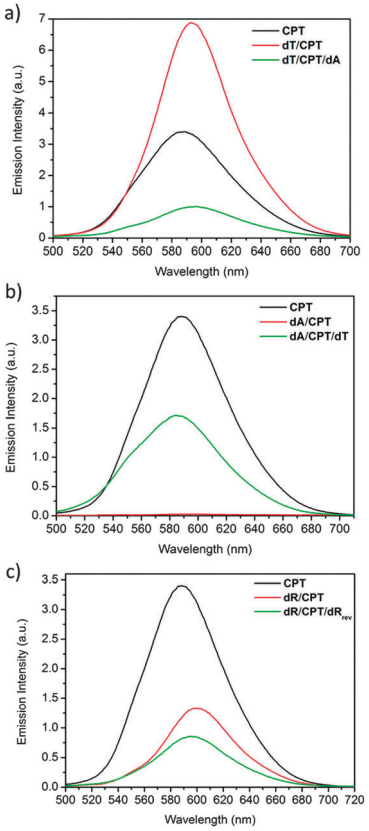

Fig. 7 Emission spectra (λ_{exc} = 450 nm) of pure **CPT** (black line) and (a) **dT/CPT** at a 1 : 1 molar ratio (red line) and **dT/CPT + dA** at a 1 : 1 : 1 molar ratio (green line); (b) **dA/CPT** at a 1 : 1 molar ratio (red line) and **dA/CPT + dT** at a 1 : 1 : 1 molar ratio (green line); and (c) **dR/CPT** at a 1 : 1 molar ratio (red line) and **dR/CPT + dR$_{rev}$** at a 1 : 1 : 1 molar ratio (green line).

For all complexes, the maximum fluorescence wavelength is red-shifted compared to the pure polymer (from $\Delta\lambda$ = +5 nm up to +12 nm for **dT/CPT** and **dR/CPT**, respectively), again attesting for a change in conformation upon binding to DNA. Surprisingly, the fluorescence intensity of the **dT/CPT** complex, with a maximum at 593 nm, is higher than for the pure **CPT** (λ_{max} = 588 nm), see Fig. 7a. This arises from the folded conformation of the pure polymer in water, which leads to "self-quenched" fluorescence.[19,23] It then turns into a more extended helical conformation around **dT**, this conformation shows enhanced emission compared to the folded **CPT**. For **dA/CPT**, however, the fluorescence of the polymer is totally quenched upon binding to **dA** at a 1 : 1 molar ratio, as a result of the strong interactions between **CPT** and **dA**. In this complex, the polymer chains are possibly aggregated (see above) in close enough proximity, which leads to fluorescence quenching. This finding

is in good agreement with the results of Scherf *et al.*,[42] who found that the fluorescence quenching is more efficient with the guanine base, *i.e.*, a purine derivative. The fluorescence is restored when the complementary strand **dT** is added to the duplex mixture (**dA/CPT + dT**) (Fig. 7b), indicative of the formation of the hybridized dsDNA/**CPT** 'triplex' structure.[3,31] In contrast, the fluorescence study using mixed sequences **dR** or $\mathbf{dR_{rev}}$ shows that the fluorescence of **CPT** is not totally quenched when binding to either **dR** or $\mathbf{dR_{rev}}$. Upon the addition of the complementary strand (**dR/CPT + dR**$_{rev}$ or $\mathbf{dR_{rev}}$**/CPT + dR**), the fluorescence intensity is somewhat lower than for **dR/CPT** or $\mathbf{dR_{rev}}$**/CPT** (Fig. 7c and Fig. S13†). This behavior is intermediate between the two previous cases, **dT/CPT + dA** and **dA/CPT + dT**, consistent with the purine/pyrimidine mixed content of the strands. This is in line with studies reported by Leclerc *et al.*, who observed very different detection properties in label-free DNA/cationic polythiophene biosensing experiments for a series of more than 50 oligonucleotides, and the variations in the spectra were attributed to the differences in conformational changes of the polymer chain with repeated DNA sequence patterns.[22]

To further decipher the differences in the biosensing mechanism and sensitivity, UV-Vis and CD spectroscopy measurements were carried out during hybridization experiments. Upon the addition of one equivalent of complementary single-stranded DNA **dA** to the **dT/CPT** polyplex (**dT/CPT + dA**), we observe the characteristic CD bands for a hybridized DNA **dA·dT** duplex, *i.e.* a positive double-peak CD signal at about 260–280 nm, a negative CD band at 248 nm, a CD band at 220 nm with a shoulder at around 238 nm, see Fig. 8a. The pronounced intensity of the ICD in the polymer region as observed for **dT/CPT** diminishes upon addition of **dA**, and the zero-crossing of the ICD signal is accordingly blue-shifted from 509 nm to 444 nm (see Fig. S14†). The UV-Vis spectra of this dsDNA/polythiophene triplex (**dT/CPT + dA**) show a maximum absorption blue-shifted compared to the duplex **dT/CPT** (see Table 1 and Fig. S14†). This is in line with what we observed with **dT·dA/CPT**, that is to say that the polymer chains present in the triplex (**dT/CPT + dA**) are less planar than in the ssDNA/**CPT** complex (**dT/CPT**), as observed for other DNA/**CPT** systems.[3,31]

The reverse hybridization process was also studied, *i.e.*, we considered a **dA/CPT** polyplex on which a complementary DNA strand **dT** is added (**dA/CPT + dT**). Surprisingly, the CD spectra of **dT/CPT + dA** and **dA/CPT + dT** are very different (Fig. 8a): no ICD signal is observed for the latter, and the CD signal in the DNA region is characteristic of pure oligoadenines **dA**. Together with the experiments and simulations on **dA/CPT** complexes, these results show that the complexation of the polymer with homopurine (**dA**) oligonucleotides yields strongly-bound complexes compared to the complexation with homopyrimidine (**dT**) bases. Upon the addition of complementary **dT**, **dA/CPT** strongly-bound complexes do not dissociate: the CD signal in the region 250–300 nm is typical of pure **dA**, not of the preformed **dA·dT** duplex (Fig. S15†). Therefore, in the **dA/CPT + dT** hybridization experiment, the **dA·dT** duplex (double-stranded DNA) does not form, while it is formed in the **dT/CPT + dA** system. These results show that the DNA–DNA hybridization experiments in the presence of CPEs can yield different polyelectrolyte aggregates depending on the working sequence of the test, which hints towards non-equilibrium mixtures.

For the **dR** and $\mathbf{dR_{rev}}$ sequences (composed of a mixed sequence of purine and pyrimidine bases), after the addition of the complementary strand to **dR/CPT** (**dR/CPT + dR**$_{rev}$) and $\mathbf{dR_{rev}}$**/CPT** ($\mathbf{dR_{rev}}$**/CPT + dR**), the CD experiments show CD spectra identical to that of **dR·dR**$_{rev}$ in the DNA region, which indicates that the DNA duplex is formed. We observe a bisignate (−/+) ICD band in the polymer region reminiscent of that in the complexation experiment **dR·dR**$_{rev}$ **+ CPT** (Fig. 8b and Fig. S16†).

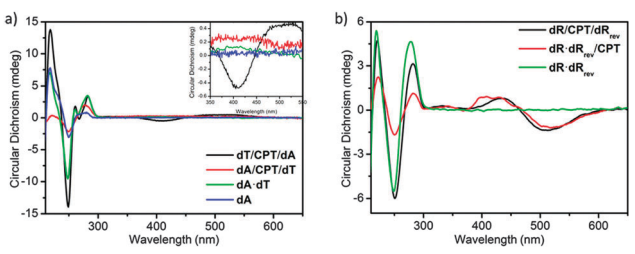

Fig. 8 Hybridization experiments: (a) CD spectra and (inset) zoom of CD spectra of the **dT/CPT + dA** triplex (black line), **dA/CPT + dT** triplex (red line), pure **dA·dT** (green line), and pure **dA** (blue line). (b) CD spectra of **dR/CPT +** $\mathbf{dR_{rev}}$ (black line), **dR·dR**$_{rev}$**/CPT** (red line) and pure **dR·dR**$_{rev}$ (green line).

DNA melting: complexation *versus* (de)hybridization

One important factor that is related to the hybridization process and reflects the stability of DNA duplexes is the melting temperature. For hybridization biosensors, the presence of the polymer can largely affect the stability of the DNA duplexes. In this view, we carried out temperature melting experiments (rate of 1 °C min^{-1} from 20 °C to 70 °C) on a series of ssDNA/**CPT** and hybridized dsDNA/**CPT** 'triplex' structures, which can give clues on the stability of the self-assembled structures. We then slowly decreased the temperature at a rate of 1 °C min^{-1} from 70 °C to 20 °C in order to allow equilibration. Interestingly, when starting from **dT/CPT + dA** (*i.e.*, a system forming **dA·dT** duplexes, see above), and heating up to 70 °C (the melting temperature (T_m) of **dA·dT** is ∼45 °C), the positive ICD signal at 530 nm becomes negative with increasing temperature (starting at around T_m), with the highest intensity recorded after the heating–cooling (H–C) cycle, see Fig. 9a and b and Fig. S17–S19.† Upon cooling, we observe an intense (−/+) ICD signal in the region where the polymer absorbs, suggesting a re-organization of the polymer chains within the complexes upon the H–C cycle. The CD signal in the 210–300 nm range also changes upon heating the mixture to 70 °C, showing a negative band at 260–280 nm, which is opposite to the signal of a right-handed B-type DNA helix. Besides, we observe a weak positive band at 300–350 nm. This CD spectrum is reminiscent of those observed in some protein-DNA structures and referred to as 'psi-aggregate' (psi or ψ for polymer–salt induced), which shows an enhancement of the ellipticity from 260 to 280 nm, and a broad band in the region 300–350 nm.[43–46] This atypical

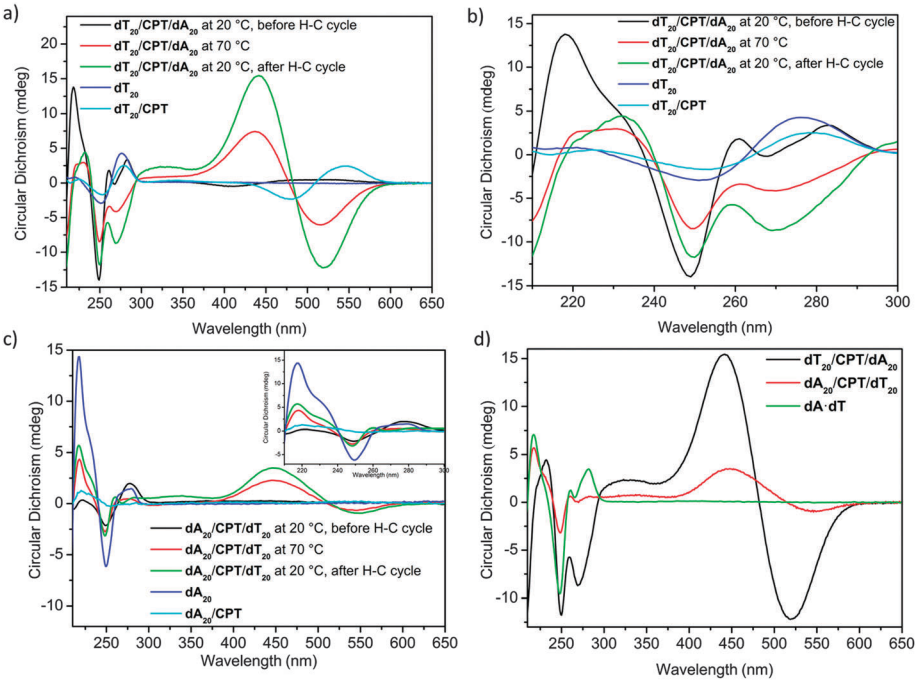

Fig. 9 Melting experiments: (a and b) CD and zoom of the CD spectra of **dT/CPT + dA** and (c) **dA/CPT + dT** at a 1 : 1 : 1 molar ratio at different temperatures. (d) Comparison of the CD spectra at a 1 : 1 : 1 molar ratio: **dT/CPT + dA** (black line), the **dA/CPT + dT** triplex (red line), pure **dA·dT** (green line) at 20 °C after the heat–cool (H–C) cycle.

CD spectrum compared to that of B-type DNA is also observed for DNA in the presence of polymers with a high concentration of salt (especially multivalent cations), cationic lipids, or alcohols, and it is a signature of a super-condensed, compactly-ordered DNA.[44–47] Clearly, the CD spectrum of the annealed **dT/CPT + dA** complex suggests that the complexes adopt an ordered form with a condensed DNA.

A heating–cooling cycle was performed on **dT/CPT + dA** with a slower rate of 0.5 °C min^{-1}. The CD spectra obtained show that the sign of the CD signals remains the same as for the cycle at 1 °C min^{-1} (*i.e.*, bisignate (+/−) ICD before heating, and (−/+) ICD after cooling), see Fig. S20.† However, the intensities of the ICD signatures are much weaker at 0.5 °C min^{-1}, which shows the effect of the H–C conditions in melting experiments.

For the reverse hybridization process **dA/CPT + dT**, the variable-temperature study shows the appearance of an ICD effect with a negative band at the lowest energy, around 35 °C. Close to 50 °C, the negative ICD band has a maximum intensity and the band at 260–280 nm shows a transition from the (+) to (−) signal (Fig. S21†). At a higher temperature (70 °C), the ICD signal decreases back to the intensity obtained at 35 °C (red line in Fig. 9c). The CD spectra measured at 20 °C after the melting study show a negative CD band in the range 260–280 nm and an ICD band, with a red-shifted zero-crossing when compared to the **dT/CPT + dA** sequence (Fig. 9d). The corresponding UV-Vis studies are in a good agreement with the appearance of the ICD, as we observe a red-shifted absorption maximum band ($\Delta\lambda_{max} \sim +18$ nm) upon the addition of the complementary strand in the mixture (see Table 1 and Fig. S21†). Altogether, the variable-temperature CD spectra for both **dT/CPT + dA** and **dA/CPT + dT** sequences show bisignate ICD with a negative band at lower energy in the polymer region (Fig. 9d), with a large difference in intensity. The CD signals are also quite different in the region 210–300 nm, with bands of opposite sign in the 260–280 nm range. In this particular case of **dA/dT**-based complexes, the heating/cooling experiments can yield different aggregates depending on the working sequence of the experiment and the rate of the temperature ramp, which shows that non-equilibrium mixtures are formed in this particular case.

After hybridization experiments of **dR·dR$_{rev}$**, upon heating the mixtures to 70 °C, *i.e.* above the melting temperature of **dR·dR$_{rev}$** ($T_m \sim 56$ °C), the CD signals for both **dR/CPT + dR$_{rev}$** and **dR$_{rev}$/CPT + dR** triplexes gradually diminish (Fig. 10), with rather small changes in the shape and position of the bands, and the UV-Vis bands remain stable with temperature (Fig. S21†). When the mixture is cooled down to 20 °C, the intensity of both the CD and UV-Vis bands is similar to those before the melting process (Fig. 10 and Fig. S22 and S23†), In this case, the hybridization process is the same whatever the order of addition, *i.e.*, from a spectroscopic point of view, we obtain the same dsDNA–**CPT** structures for **dR/CPT + dR$_{rev}$** and **dR$_{rev}$/CPT + dR**, with a left-handed polymer helical assembly in all cases (Fig. 10c). Moreover, the UV-Vis and CD spectra are identical before and after cooling, which demonstrates that stable assemblies are formed before the melting studies. Altogether, the DNA/**CPT** self-assembly in these mixed sequences shows a marked behavior, compared to that of homonucleotide sequences, indicating again the strong differences in the hybridization process depending on the purine/pyrimidine ratio in the DNA sequence.

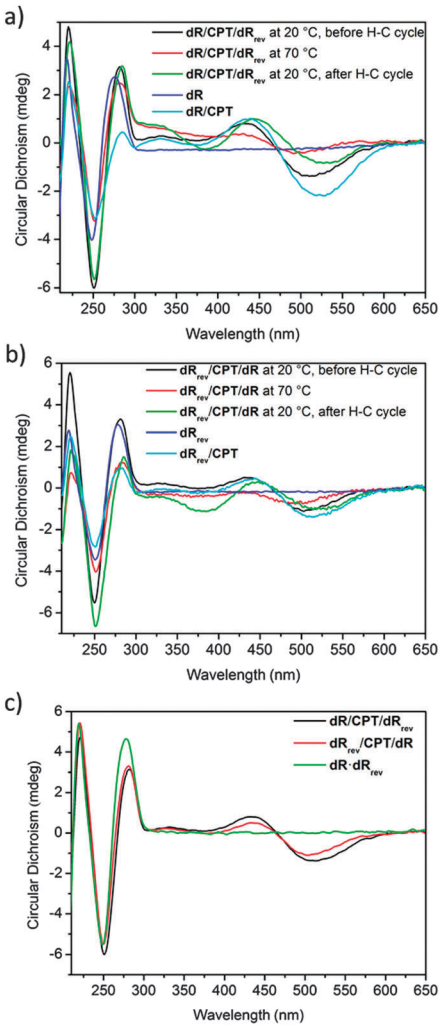

Fig. 10 Melting experiments: (a) CD spectra of **dR/CPT + dR$_{rev}$** and (b) **dR$_{rev}$/CPT + dR** at a 1:1:1 molar ratio at different temperatures. (c) Comparison of the CD spectra at 20 °C after the heat–cool (H–C) cycle: **dR/CPT + dR$_{rev}$** (black line), **dR$_{rev}$/CPT + dR** (red line), pure **dR·dR$_{rev}$** (green line).

Conclusions

We have shown that the self-assembly between DNA and **CPT** in aqueous buffered solution strongly depends on the DNA sequence, length, and topology, as related to a subtle balance between electrostatic and π-type intermolecular interactions. Especially, the CD signatures of DNA/**CPT** complexes vary substantially with the oligonucleotide sequence. For homo-nucleotide sequences (**dT** or **dA**), the complexation between ssDNA and **CPT** leads to a preferential right-handed conformation of the polymer chain, and molecular modelling pinpoints the structural and interactional differences related to the nature of the nucleobase. In contrast, **CPT** complexation with oligo-nucleotides of a mixed sequence (in ssDNA or dsDNA topologies) gives rise to left-handed ICD signatures. This is an unexpected result in view of the higher propensity for the polymer chains to bind into the minor grooves of the double strand DNA and thereby adopt a right-handed helical conformation. It likely hints towards the role of aggregation effects, though more systematic investigations possibly supported by coarse-grained models are definitively needed to sort it out. We have also demonstrated that the hybridization mechanism is highly dependent on the sequence of the biosensing experiment, because the formation of certain strongly-bound ssDNA/**CPT** complexes affects further DNA duplex formation. The melting temperature experiments show that specific dsDNA/**CPT** 'triplexes' can yield super-condensed DNA structures *via* the formation of psi-aggregates. These studies also show that non-equilibrium mixtures can form, especially for hybridization/melting experiments using the homopurine/homopyrimidine complex (**dA/dT/CPT**), depending on the working sequence of the experiment and heating/cooling conditions. Altogether, these results provide clues on the self-assembly, stability, and structural aspects of DNA/π-conjugated polyelectrolyte complexes, which are of major interest for prospective biomedical applications in DNA sensing and in gene-delivery polyplexes.

Acknowledgements

The authors thank Pol Boudard for a preliminary work on molecular models. This work was supported by the Fonds de la Recherche Scientifique – FNRS under the grant BINDER no. 2.4615.11. Research in Mons is also supported by the Excellence Pole program of Région Wallonne (OPTI2MAT project), the Science Policy Office of the Belgian Federal Government (PAI 7/5) and FNRS-FRFC. J.R.-M., D.B., and M.S. are FNRS researchers. S.K. is grateful to the European Marie Curie (COFUND) programme and the Belgian Science Policy Office (BELSPO). The authors also thank CNRS and the Université de Montpellier for financial support.

Notes and references

1 *Conjugated Polyelectrolytes. Fundamentals and Applications*, ed. B. Liu and G. C. Bazan, Wiley-VCH, 2013.
2 J. Liang, K. Li and B. Liu, *Chem. Sci.*, 2013, **4**, 1377.
3 H.-A. Ho, M. Boissinot, M. G. Bergeron, G. Corbeil, K. Doré, D. Boudreau and M. Leclerc, *Angew. Chem., Int. Ed.*, 2002, **41**, 1548–1551.
4 K. P. R. Nilsson and O. Inganäs, *Nat. Mater.*, 2003, **2**, 419–424.
5 H.-A. Ho, A. Najari and M. Leclerc, *Acc. Chem. Res.*, 2008, **41**, 168–178.
6 P. Hammarström, R. Simon, S. Nystrom, P. Konradsson, A. Aslund and K. P. Nilsson, *Biochemistry*, 2010, **49**, 6838–6845.
7 P. Bjork, A. Herland, M. Hamedi and O. Inganäs, *J. Mater. Chem.*, 2010, **20**, 2269–2276.
8 T. Klingstedt, H. Shirani, K. O. A. Åslund, N. J. Cairns, C. J. Sigurdson, M. Goedert and K. P. R. Nilsson, *Chem. – Eur. J.*, 2013, **19**, 10179–10192.
9 F. Xia, X. Zuo, R. Yang, Y. Xiao, D. Kang, A. Vallée-Bélisle, X. Gong, A. J. Heeger and K. W. Plaxco, *J. Am. Chem. Soc.*, 2010, **132**, 1252–1254.

10 C. Chi, A. Mikhailovsky and G. C. Bazan, *J. Am. Chem. Soc.*, 2007, **129**, 11134–11145.
11 J. W. Hong, W. L. Hemme, G. E. Keller, M. T. Rinke and G. C. Bazan, *Adv. Mater.*, 2006, **18**, 878–882.
12 B. S. Gaylord, A. J. Heeger and G. C. Bazan, *Proc. Natl. Acad. Sci. U. S. A.*, 2002, **99**, 10954–10957.
13 F. Xia, X. Zuo, R. Yang, Y. Xiao, D. Kang, A. Vallée-Bélisle, X. Gong, J. D. Yuen, B. B. Y. Hsu, A. J. Heeger and K. W. Plaxco, *Proc. Natl. Acad. Sci. U. S. A.*, 2010, **107**, 10837–10841.
14 M. Béra-Abérem, A. Najari, H. A. Ho, J. F. Gravel, P. Nobert, D. Boudreau and M. Leclerc, *Adv. Mater.*, 2006, **18**, 2703–2707.
15 B. Liu and G. C. Bazan, *Chem. Mater.*, 2004, **16**, 4467–4476.
16 B. S. Gaylord, M. R. Massie, S. C. Feinstein and G. C. Bazan, *Proc. Natl. Acad. Sci. U. S. A.*, 2005, **102**, 34–39.
17 X. Feng, L. Liu, S. Wang and D. Zhu, *Chem. Soc. Rev.*, 2010, **39**, 2411–2419.
18 X. Duan, L. Liu, F. Feng and S. Wang, *Acc. Chem. Res.*, 2010, **43**, 260.
19 Z. Liu, H.-L. Wang and M. Cotlet, *Chem. Mater.*, 2014, **26**, 2900–2906.
20 H. A. Ho, K. Doré, M. Boissinot, M. G. Bergeron, R. M. Tanguay, D. Boudreau and M. Leclerc, *J. Am. Chem. Soc.*, 2005, **127**, 12673–12676.
21 B. Liu and G. C. Bazan, *Proc. Natl. Acad. Sci. U. S. A.*, 2005, **102**, 589–593.
22 I. Charlebois, C. Gravel, N. Arrad, M. Boissinot, M. G. Bergeron and M. Leclerc, *Macromol. Biosci.*, 2013, **13**, 717–722.
23 Z. Liu, H.-L. Wang and M. Cotlet, *Chem. Commun.*, 2014, **50**, 11311–11313.
24 C. Zhu, L. Liu, Q. Yang, F. Lv and S. Wang, *Chem. Rev.*, 2012, **112**, 4687–4735.
25 A. C. Carreon, W. L. Santos, J. B. Matson and R. C. So, *Polym. Chem.*, 2014, **5**, 314–317.
26 G. Yang, H. Yuan, C. Zhu, L. Liu, Q. Yang, F. Lv and S. Wang, *ACS Appl. Mater. Interfaces*, 2012, **4**, 2334–2337.
27 J. Rubio-Magnieto, A. Thomas, S. Richeter, A. Mehdi, P. Dubois, R. Lazzaroni, S. Clément and M. Surin, *Chem. Commun.*, 2013, **49**, 5483–5485.
28 J. D. Winter, G. Deshayes, F. Boon, O. Coulembier, P. Dubois and P. Gerbaux, *J. Mass Spectrom.*, 2011, **46**, 237–246.
29 S. Samitsu, T. Shimomura, S. Heike, T. Hashizume and K. Ito, *Macromolecules*, 2008, **41**, 8000–8010.
30 S. Burge, G. N. Parkinson, P. Hazel, A. K. Todd and S. Neidle, *Nucleic Acids Res.*, 2006, **34**, 5402–5415.
31 H.-A. Ho, M. Béra-Abérem and M. Leclerc, *Chem. – Eur. J.*, 2005, **11**, 1718–1724.
32 M. Knaapila, T. Costa, V. M. Garamus, M. Kraft, M. Drechsler, U. Scherf and H. D. Burrows, *Macromolecules*, 2014, **344**, 491.
33 C. Chi, A. Chworos, J. Zhang, A. Mikhailovsky and G. C. Bazan, *Adv. Funct. Mater.*, 2008, **18**, 3606–3612.
34 K. P. Nilsson, J. Rydberg, L. Baltzer and O. Inganäs, *Proc. Natl. Acad. Sci. U. S. A.*, 2004, **101**, 11197–11202.
35 M. Surin, P. G. A. Janssen, R. Lazzaroni, Ph. Leclère, E. W. Meijer and A. P. H. J. Schenning, *Adv. Mater.*, 2009, **21**, 1126–1130.
36 A. Digennaro, H. Wennemers, G. Joshi, S. Schmid, E. Mena-Osteritz and P. Bäuerle, *Chem. Commun.*, 2013, **49**, 10929–10931.
37 *Comprehensive Chiroptical Spectroscopy. Applications in Stereochemical Analysis of Synthetic Compounds, Natural Products, and Biomolecules*, ed. N. Berova, P. L. Polavarapu, K. Nakanishi and R. W. Woody, United States of America, 2012.
38 H. Qiu, J. B. Gilroy and I. Manners, *Chem. Commun.*, 2013, **49**, 42–44.
39 S. Stella, D. Cascio and R. C. Johnson, *Genes Dev.*, 2010, **24**, 814–826.
40 P. L. Privalov, A. I. Dragan, C. Crane-Robinson, K. J. Breslauer, D. P. Remeta and C. A. S. A. Minetti, *J. Mol. Biol.*, 2007, **365**, 1–9.
41 L. Yang, M. Zhao, R. Zhang, J. Dong, T. Zhang, X. Zhan and G. Wang, *ChemPhysChem*, 2012, **13**, 4099–4104.
42 M. L. Davies, P. Douglas, H. D. Burrows, B. Martincigh, M. da Graca Miguel, U. Scherf, R. Malavia and A. Douglas, *J. Phys. Chem. B*, 2014, **118**, 460.
43 S. Osfouri, P. Stano and P. L. Luisi, *J. Phys. Chem. B*, 2005, **109**, 19929–19935.
44 G. D. Fasman, *Circular Dichroism and the Conformational. Analysis of Biomolecules*, Plenum Press, New York, 1996.
45 A. V. Pietrini and P. L. Luisi, *Biochim. Biophys. Acta*, 2002, **1562**, 57–62.
46 B. I. Kankia, V. Buckin and V. A. Bloomfield, *Nucleic Acids Res.*, 2001, **29**, 2795–2801.
47 V. A. Bloomfield, *Biopolymers*, 1997, **44**, 269–282.